

Superconductivity and phase separation in electrochemically hydrogenized $K_{1-\delta}Cr_3As_3H_x$ Jin-Jin Xiang,^{1,*} Ye-Ting Shao,^{1,*} Yan-Wei Cui^{①,1,2,*} Lin-Peng Nie,³ Si-Qi Wu,¹ Bai-Zhuo Li,¹ Zhi Ren,² Tao Wu,³ and Guang-Han Cao^{①,4,5,†}¹Department of Physics, Zhejiang University, Hangzhou 310027, China²School of Sciences, Westlake Institute for Advanced Study, Westlake University, Hangzhou 310064, China³Hefei National Laboratory for Physical Sciences at Microscale and Department of Physics, and CAS Key Laboratory of Strongly-coupled Quantum Matter Physics, University of Science and Technology of China, Hefei, Anhui 230026, China⁴Zhejiang Province Key Laboratory of Quantum Technology and Devices, Interdisciplinary Center for Quantum Information, and State Key Lab of Silicon Materials, Zhejiang University, Hangzhou 310027, China⁵Collaborative Innovation Centre of Advanced Microstructures, Nanjing University, Nanjing 210093, China

(Received 22 September 2020; accepted 30 November 2020; published 15 December 2020)

We report preparation, crystal structure, and physical properties of a quasi-one-dimensional Cr-based arsenide hydride $K_{1-\delta}Cr_3As_3H_x$. Through an electrolysis using essentially nonsuperconducting samples as the cathode, additional hydrogen atoms can be successfully intercalated up to $x = 0.45$ and, consequently, the in-plane and interplane Cr–Cr bond distances in the chains of face-sharing Cr octahedra increase by 3.7% and 1.5%, respectively. The electrochemically hydrogenized samples show a broad superconducting transition at $T_c = 5.8$ K, a record in the K–Cr–As–H system, with nearly full magnetic shielding at 1.8 K. The electronic specific-heat coefficient extracted from the specific-heat measurement is as high as $\gamma_n = 47$ mJ K^{−2} mol Cr^{−1}, suggesting a stronger electron correlation that is likely to be associated with the expansions of Cr–Cr bonds. Meanwhile, the dimensionless specific-heat jump $\Delta C/(\gamma_n T_c)$ is only 0.30, about 20% of the expected value in the BCS weak-coupling scenario. Furthermore, the normal-state magnetism is characterized by Curie-Weiss paramagnetism with an enhanced effective localized moment of 1.33 μ_B /Cr, suggesting that a nonsuperconducting phase with localized spins dominates. The ¹H nuclear magnetic resonance measurement reveals two different spin-lattice relaxations, corresponding to superconducting and localized-spin phases, respectively. All the results point to phase separation with minority superconducting phase and majority nonsuperconducting phase in the quasi-one-dimensional $K_{1-\delta}Cr_3As_3H_x$ system.

DOI: [10.1103/PhysRevMaterials.4.124802](https://doi.org/10.1103/PhysRevMaterials.4.124802)

I. INTRODUCTION

Recent discovery of superconductivity (SC) in quasi-one-dimensional (Q1D) $K_2Cr_3As_3$ provided a rare example that SC occurs in Q1D correlated-electron systems [1]. The Q1D character is represented by the linear $[(Cr_3As_3)^{2-}]_\infty$ chains that are separated apart with K counterions. The superconducting transition temperature T_c is 6.1 K at ambient pressure, which is about three times of the T_c value of CrAs under high pressures [2]. The electronic specific-heat coefficient in the normal state γ_n is about 24 mJ K^{−2} mol Cr^{−1} [1,3,4], also nearly three times of that of CrAs [5]. Importantly, the γ_n value is about four times of the calculated one from the first-principles calculations [6], suggesting significant electron correlations in $K_2Cr_3As_3$. Evidence for possible spin-triplet unconventional superconductivity is accumulating in the Q1D Cr-based system [7–13].

The Q1D Cr-based material has been extended into several specific compounds in two categories. With the elemental replacement at the K site, first, three additional members in the $A_2Cr_3As_3$ ($A = Na, K, Rb, \text{ and } Cs$) family were subsequently discovered [14–16]. All these so-called 233-type

materials are superconductors. The T_c values of $A_2Cr_3As_3$ are 4.8, 2.2, and 8.6 K, respectively, for $A = Rb, Cs, \text{ and } Na$. Noticeably, T_c roughly scales with γ_n [7], implying the relevance and importance of electron correlations. Second, with a topotactic deintercalation reaction, one was able to obtain 133-type compounds ACr_3As_3 ($A = K, Rb, \text{ and } Cs$) which remain the $(Cr_3As_3)_\infty$ chains [17,18]. The pristine 133-type polycrystalline samples were not superconducting, instead a cluster-spin-glass state appears below ~ 5 K [17–19].

Surprisingly, in contrast with the nonsuperconducting behavior of KCr_3As_3 polycrystals, the “ KCr_3As_3 ” single crystals, especially those after a post treatment in ethanol bath, were reported to exhibit SC at $T_c^{\text{onset}} = 3.7\text{--}4.7$ K [20]. The present authors later found that the pristine KCr_3As_3 single crystals were nonsuperconducting also, and SC was actually induced by aging and/or annealing [21]. Taddei *et al.* [22] revealed that intercalation of hydrogen plays the crucial role for the appearance of SC. The incorporated H atom locates at the center of Cr octahedra in the $(Cr_3As_3)_\infty$ chains. This means that the H intercalation needs to overcome an energy barrier of the $(Cr_3As_3)_\infty$ double-walled subnanotubes [1], which explains the aging and annealing effect [21]. A theoretical investigation based on the first-principles calculations [23] indicates that the intercalated H atom acts as an electron acceptor, i.e., the hydrogen is basically in the form of H[−]

*These authors contributed equally to this work.

†ghcao@zju.edu.cn

hydride ions. The hydrogen strongly bonds with the surrounding Cr atoms, giving rise to a nontrivial electron doping. Consequently, the band filling is close to that of $\text{K}_2\text{Cr}_3\text{As}_3$, which could be the reason for the emergence of SC.

There is an important issue on the superconducting volume fraction (SVF) of the post-treated superconducting “ KCr_3As_3 ” single crystals [20] and $\text{KCr}_3\text{As}_3\text{H}_x$ polycrystals [21,22]. Although the magnetic shielding fraction (MSF), measured in the zero-field-cooling (ZFC) mode, could be near 100% [20], the dimensionless specific-heat jump of the superconducting “ KCr_3As_3 ” crystals was only about 20% of that of $\text{K}_2\text{Cr}_3\text{As}_3$, suggesting nonbulk nature of the SC observed. The result is probably due to the limited H intercalation using the aging and annealing strategy [21]. It is of great interest to develop a more effective way for H intercalation, and then to directly investigate the effect of the H intercalation in the $\text{KCr}_3\text{As}_3\text{H}_x$ system.

Here we report that additional hydrogen can be intercalated into $\text{K}_{1-\delta}\text{Cr}_3\text{As}_3\text{H}_x$ samples up to $x = 0.45$ via an electrochemical hydrogenization in KOH solution at $\sim 75^\circ\text{C}$. The H intercalation obviously expands the face-sharing Cr-octahedron chains. Meanwhile, the T_c value is increased up to 5.8 K, which is a record in the K-Cr-As-H system. Although the superconducting sample shows nearly 100% MSF, the dimensionless specific-heat jump at T_c is merely 0.30, about 20% of the theoretically expected value and 13% of that of 233-type $\text{K}_2\text{Cr}_3\text{As}_3$, indicating a minority of superconducting phase in the sample. The majority phase exhibits Curie-Weiss (CW) paramagnetism with an enhanced effective magnetic moment from Cr localized electrons. The electronic inhomogeneity is also supported by the ^1H NMR measurement which reveals two different spin-lattice relaxations corresponding to SC and localized spins, respectively. We also observed an enhanced electronic specific-heat coefficient, suggesting a stronger electron correlation that could be associated with the Cr-lattice expansions because of H intercalation.

II. EXPERIMENT

Preparation of $\text{K}_{1-\delta}\text{Cr}_3\text{As}_3\text{H}_x$. The pristine H-poor $\text{K}_{1-\delta}\text{Cr}_3\text{As}_3\text{H}_x$ samples were prepared using a soft-chemical deintercalation reaction of $\text{K}_2\text{Cr}_3\text{As}_3$ polycrystals, similar to the previous reports [17,21]. $\text{K}_2\text{Cr}_3\text{As}_3$ polycrystals were synthesized by solid-state reactions in vacuum, according to Ref. [1]. The values of δ and x can be controlled to some extent by aging or annealing in ethanol [21]. For the electrolysis purpose in this work, samples of $\text{K}_{1-\delta}\text{Cr}_3\text{As}_3\text{H}_x$ with $\delta = 0-0.1$ and $x = 0.2-0.35$ were employed. As shown in Fig. S2 of the Supplemental Material (SM) [24], these samples do not show SC, or show only trace SC, above 1.8 K.

Electrochemical hydrogenization. The hydrogenization was realized by an electrolysis, instead of aging and annealing in previous works [20–22]. The electrolysis, with the experimental setup shown in Fig. S1 of SM [24], employed a three-electrode approach. The unhydrogenized $\text{K}_{1-\delta}\text{Cr}_3\text{As}_3\text{H}_x$ sample, cut into a bar, was adhered to platinum wire with silver paste. KOH solution was chosen as the electrolyte, which was heated with a water bath. A calomel electrode (Lei Ci 232-01) was used as the reference electrode.

The electrolysis was carried out on an electrochemical workstation either at steady potential or at constant current mode.

To optimize the condition for electrochemical hydrogenization, we performed several controlled experiments with the considerations of (1) electrolysis temperature, (2) total electric quantity, and (3) electrolyte concentration. The detailed results can be seen in the SM [24]. We found that the electrolysis at an elevated temperature of $\sim 75^\circ\text{C}$ with excess amount of electricity passed through the electrolysis cell could reproducibly obtain a good hydrogenized sample of $\text{K}_{1-\delta}\text{Cr}_3\text{As}_3\text{H}_x$ with $\delta \approx 0-0.1$ and $x \approx 0.45$ which shows relatively high T_c and high MSF.

Structural and compositional characterizations. Powder x-ray diffraction (XRD) experiments were carried out on a PANalytical x-ray diffractometer (Empyrean) at room temperature with a monochromatic $\text{CuK}\alpha_1$ radiation. For the purpose of a Rietveld refinement, the XRD data were collected with a slow scan ($0.5^\circ/\text{min}$) from $2\theta = 5^\circ$ to 150° . The chemical composition of the crystallites was measured using energy-dispersive x-ray spectroscopy (EDS). The EDS data were collected with an Octane Plus Detector (AMETEX EDAX) equipped in a field-emitting scanning electron microscope (SEM, Hitachi S-4800). Line scans were performed to investigate the possible compositional inhomogeneity. The atomic percentages of K, Cr, and As were obtained using the K lines by the eZAF Smart Quant analysis. The H content was measured by the ^1H nuclear magnetic resonance (NMR) as described below. More details are presented in Sec. III of the SM [24].

Physical property measurements. Electrical resistivity and heat capacity were measured using a standard four-probe method and a relaxation technique, respectively, on a Quantum Design physical property measurement system (PPMS-9). The dc magnetic susceptibility was measured on a Quantum Design magnetic property measurement system (MPMS3). For detecting the superconducting transition, both the ZFC and field-cooling (FC) protocols were employed under a low field of 10 Oe. For the measurement of the normal-state susceptibility, a high field of 10 kOe was applied.

NMR measurements. The NMR spectra were obtained by the FFT (fast Fourier transformation) sum of the standard spin-echo signals which were carried out on commercial NMR spectrometer from Thamway Co. Ltd. with the external magnetic field generated by a 12-T magnet from Oxford Instruments. To reduce the ^1H signal from the background, the insulation layer of NMR coil was removed. The polycrystalline sample and glycerol power as the standard sample were sealed in two same capillary silica tubes under the argon atmosphere in the glove box, respectively. With identical measurement condition for target sample and standard sample, we could estimate the hydrogen content in the target sample by comparing the integral area of ^1H NMR spectrum between target sample and standard sample. Details can be found in the SM [24]. The nuclear spin-lattice relaxation rate ($1/T_1$) was measured by recording the recovery curve after saturation comb. In this study, the recovery curve of the nuclear magnetization $M(t)$ shows an obvious two-component behavior, which is fitted with the formula

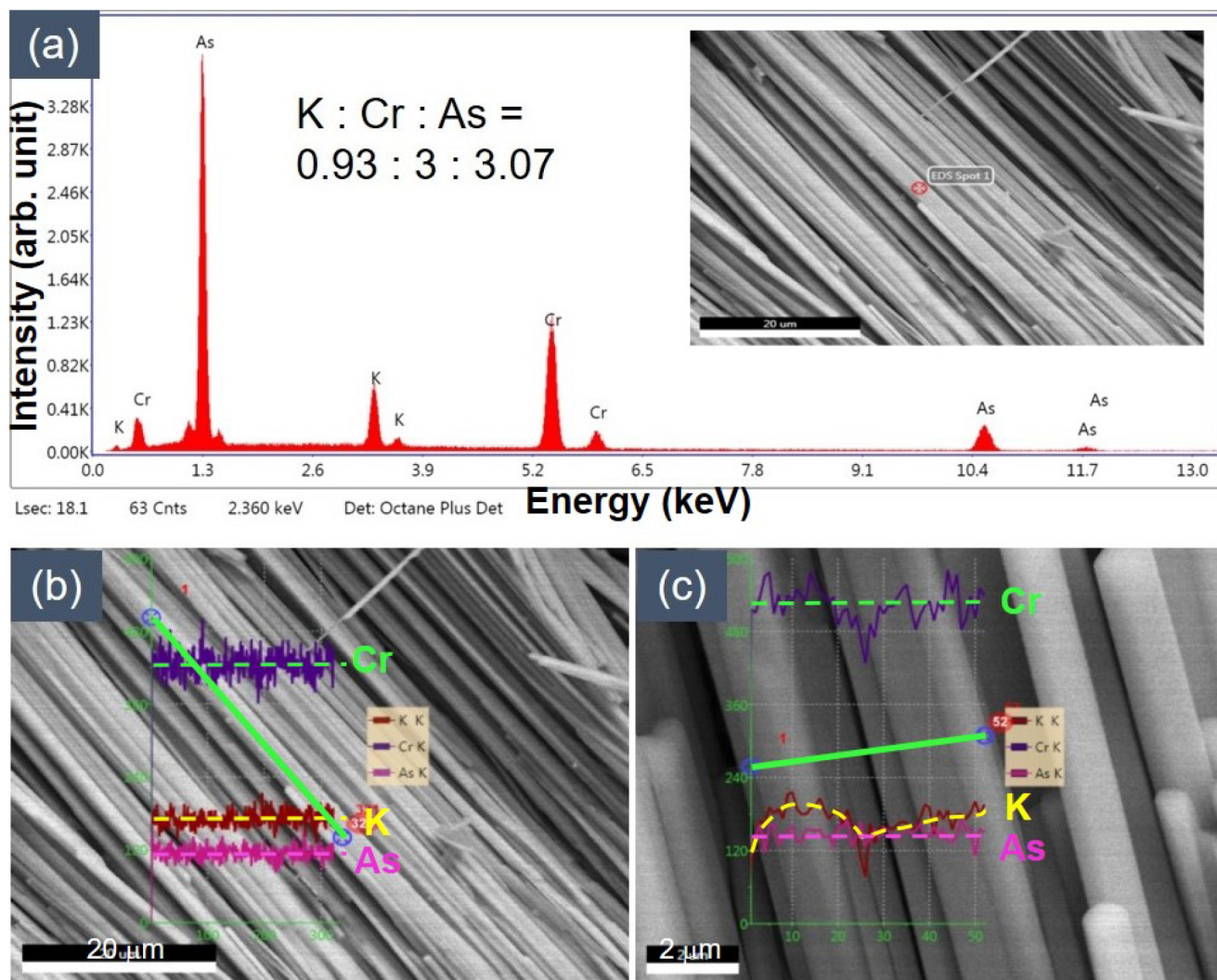


FIG. 1. Chemical composition analysis for the electrochemically hydrogenized $K_{1-\delta}Cr_3As_3H_x$ sample using energy-dispersive x-ray spectra (EDS). (a) A typical EDS with electron beam focused on a crystalline rod. (b), (c) SEM images in which EDS line scans (in bold green) along and across the aligned crystalline rods were performed. The dashed lines are guides to the eye showing variations of the chemical composition.

$$1 - \frac{M(t)}{M(\infty)} = \frac{1}{I_1 + I_2 + I_{noise}} \left\{ I_1 \exp\left[-\left(\frac{t}{T_1}\right)^{r_1}\right] + I_2 \exp\left[-\left(\frac{t}{T_2}\right)^{r_2}\right] + I_{noise} \right\},$$

and the error bars are determined by the least-square method.

III. RESULTS AND DISCUSSION

A. Composition and crystal structure

The chemical compositions of the electrochemically hydrogenized sample were analyzed using EDS. Figure 1(a) shows a typical EDS collected on the crystallite, which gives a nearly stoichiometric composition within the measurement uncertainty. The K content is statistically higher than those of long-time-aged or annealed samples [21], indicating no loss of K during the electrolysis. To investigate the possible chemical inhomogeneity, we made line scans along and across the rod

(*c*-axis) direction. As shown in Fig. 1(b), no compositional variance is evident for the scan along the rod. In the case of the scan across the rods [Fig. 1(c)], however, the K content tends to decrease at the edges of the crystallite rods (while As and Cr do not show such a variation). The result suggests that the outer part of the crystallite rods could have some K vacancies. This spatial inhomogeneity in K content is consistent with the XRD-peak broadening especially for (*hk*0) reflections in all 133-type samples [21].

The “average” crystal structure of the hydrogenized $K_{1-\delta}Cr_3As_3H_x$ was studied by laboratory XRD. Figure 2 presents the powder XRD pattern, which shows a 133-type single phase. The crystal structure was refined by the Rietveld

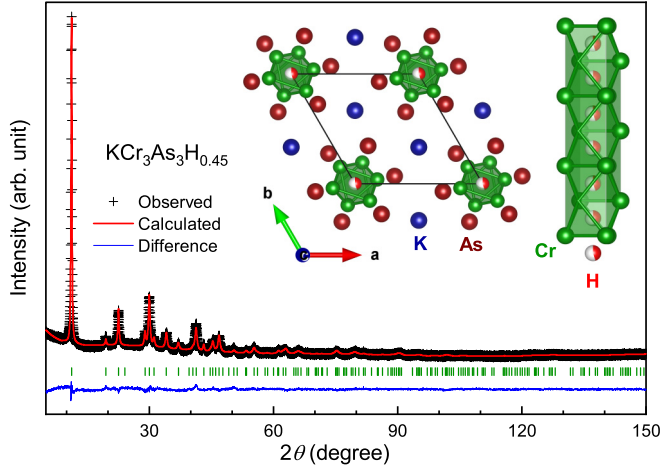


FIG. 2. Rietveld refinement profile of powder x-ray diffraction of the electrochemically hydrogenized $\text{KCr}_3\text{As}_3\text{H}_{0.45}$. The middle inset shows the crystal structure projected along the c axis. The right inset highlights the $\text{Cr}_3\text{H}_{0.45}$ face-sharing-octahedron chains with H atoms at the centers.

analysis [25] using the crystallographic data of KCr_3As_3 in Ref. [17] as the initial structure input. Irrespective of negligible contribution from hydrogen, for completeness, hydrogen atoms were included, which occupy the $2b(0,0,0)$ site [22], and the occupancy was set to 0.45 according to the ^1H -NMR measurement [24]. The occupancy of K was fast converged to 1.0 during the Rietveld refinement, although the compositional analysis above shows slight deficiency and inhomogeneity. The possible explanation is that the inner part of the crystallite rods with nearly stoichiometric K content has better crystallinity [21], which contributes most of the XRD intensities. If this is true, the “average” structure refined mainly reflects the inner part of the crystallites. This scenario is consistent with the EDS line-scan result. Considering that the K deficiency is insignificant, especially for the inner portion of the crystallites, we hereafter do not take it into account (unless specified), and the chemical formula is uniformly written as $\text{KCr}_3\text{As}_3\text{H}_{0.45}$.

As shown in Fig. 2, the refinement is very successful with a fairly low reliable factor ($R_{\text{wp}} = 5.18\%$) and an excellent value of goodness of fit ($S = 1.23$). The crystallographic data obtained are listed in Table I, which are basically consistent with those from neutron diffractions for the superconducting samples [22]. Table II compares the crystal structures be-

TABLE I. Crystallographic data of $\text{KCr}_3\text{As}_3\text{H}_x$ at room temperature refined with powder XRD. The space group is $P6_3/m$ (No. 176), and the lattice parameters are $a = 9.0975(8)$ Å and $c = 4.1910(6)$ Å. The occupancy of hydrogen was fixed to be 0.45 according to the ^1H -NMR measurement [24].

Atom	Site	x	y	z	B
K	$2c$	1/3	2/3	0.25	1.2(2)
Cr	$6h$	0.1538(6)	0.1934(4)	0.25	2.5(1)
As	$6h$	0.3453(5)	0.0701(4)	0.25	0.42(8)
H	$2b$	0.0	0.0	0.0	2(fixed)

TABLE II. Comparison of structural and physical properties of nonsuperconducting KCr_3As_3 [17] and superconducting $\text{KCr}_3\text{As}_3\text{H}_{0.45}$. The Cr–As–Cr angle is the one along the crystallographic c axis. The parameters T_c^{on} , T_{SG} , P_{eff} , θ_{CW} , and γ_n denote the superconducting onset transition temperature, glassy spin-freezing temperature, effective magnetic moment, paramagnetic Curie-Weiss temperature, and electronic specific-heat coefficient, respectively.

Parameters	KCr_3As_3	$\text{KCr}_3\text{As}_3\text{H}_{0.45}$
a (Å)	9.0909(8)	9.0975(8)
c (Å)	4.1806(2)	4.1910(6)
In-plane Cr–Cr (Å)	2.691(2)	2.791(4)
Interplane Cr–Cr (Å)	2.604(1)	2.644(3)
Cr–As–Cr ($^\circ$)	116.4(1)	117.8(2)
T_c^{on} (K)	–	5.8
T_{SG} (K)	4.5	6.5
P_{eff} (μ_B/Cr)	0.68	1.33
θ_{CW} (K)	–83	–61
γ_n ($\text{mJ K}^{-2} \text{mol Cr}^{-1}$)	20	47

tween nonsuperconducting KCr_3As_3 [17] and hydrogenized superconducting $\text{KCr}_3\text{As}_3\text{H}_{0.45}$. First of all, the lattice constants increase obviously with the hydrogenization. The a axis increases by 0.07%, and the c axis increases by 0.25%. The results qualitatively agree with those of neutron diffraction study [22]. Looking into the face-sharing Cr-octahedron chains (see the right inset of Fig. 2), one finds 3.7% increase of the in-plane Cr–Cr bond length and 1.5% increase of the interplane Cr–Cr one, which are very remarkable compared with the small increases of lattice parameters. That is to say, each Cr octahedron becomes not only larger by a few percent, but also flatter with the hydrogenization. Furthermore, the Cr–As–Cr bond angle along the c axis, which was proposed to be a crucial parameter for the magnetic exchange interactions [13], also increases by 1.2%. These structural changes are easily understood as a result of H intercalation because only Cr atoms are the nearest neighbors of the intercalated hydrogen.

B. Electrical and magnetic properties

Figure 3 shows the temperature dependence of electrical resistivity for the electrochemically hydrogenized $\text{KCr}_3\text{As}_3\text{H}_{0.45}$ polycrystalline sample. In contrast to the KCr_3As_3 polycrystals which show a semiconducting behavior [17], the hydrogenized sample exhibits a metallic conduction. The residual resistivity ratio $\rho_{300\text{K}}/\rho_{7\text{K}} \approx 4$ is even larger than that (~ 3) of the post-treated superconducting “ KCr_3As_3 ” crystals [20]. The low-temperature (7–50 K) resistivity obeys a power law $\rho = \rho_0 + AT^2$, resembling that of impurity-bearing 233-type $\text{K}_2\text{Cr}_3\text{As}_3$ crystals [26], implying dominant electron-electron scattering. A superconducting transition is clearly seen with the onset and zero-resistance temperatures at 6.0 and 5.0 K, respectively. The transition width is obviously broader than that of the 233-type polycrystals [1], suggesting possible existence of inhomogeneity and/or phase separation. Notably, the superconducting transition temperature is the highest among the 133-type K–Cr–As–H system [20–22]. Given the remarkable enhancement of T_c with hydrogenization, we speculate that the Rb-containing 133-type RbCr_3As_3

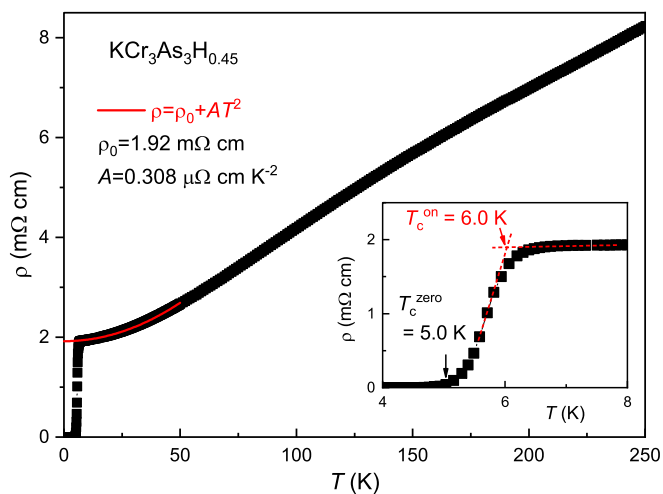


FIG. 3. Temperature dependence of electrical resistivity for the electrochemically hydrogenized $\text{KCr}_3\text{As}_3\text{H}_{0.45}$ polycrystalline sample. The red solid line gives the data fit with the formula shown. The inset displays the closeup which clearly shows the superconducting transition.

crystals, which show a higher onset T_c of 7.3 K [27], might also involve the H intercalation.

The upper critical fields [$\mu_0 H_{c2}(T)$] were obtained by the measurement of resistivity under magnetic fields up to 9 T using additional electrolytic and pristine samples of $\text{KCr}_3\text{As}_3\text{H}_x$, as shown in Fig. S9 of the SM [24]. The zero-temperature upper critical field $\mu_0 H_{c2}(0)$ was estimated to be 27 and 20 T, respectively, for the electrolytic and pristine samples [21]. Note that the samples before electrolysis do not show SC above 1.8 K, or only show trace SC with a MSF of 0.1%–0.3% (see Fig. S2 in the SM [24]). After the electrolysis even at room temperature (without annealing effect), superconductivity at 4.9 K emerges with a MSF of 100% (see Table S1 in the SM [24]). Therefore, the result directly demonstrates that H intercalation induces and enhances SC in the $\text{KCr}_3\text{As}_3\text{H}_x$ system.

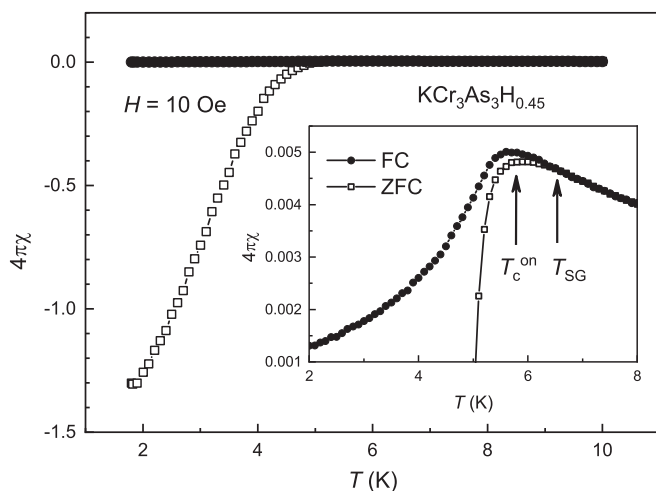


FIG. 4. Temperature dependence of dc magnetic susceptibility at low temperatures for $\text{KCr}_3\text{As}_3\text{H}_{0.45}$. FC and ZFC denote field cooling and zero-field cooling, respectively. The inset shows the closeup from which the superconducting onset transition and spin-glass transition can be simultaneously seen (marked by the arrows).

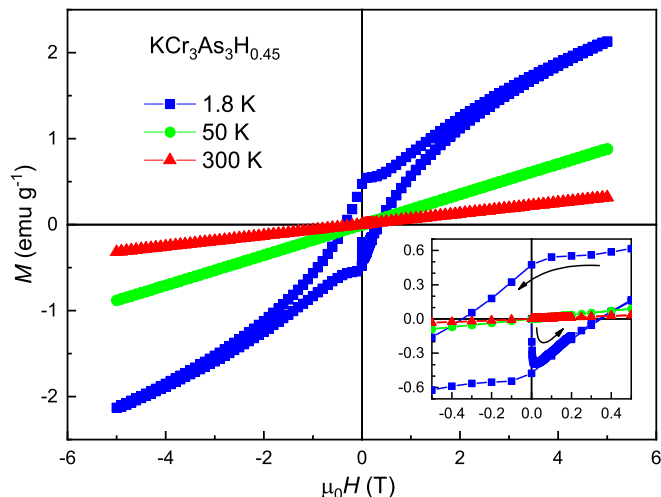


FIG. 5. Field dependence of magnetization at different temperatures for $\text{KCr}_3\text{As}_3\text{H}_{0.45}$. The inset shows the closeup at low fields.

Figure 4 shows the temperature dependence of dc magnetic susceptibility for $\text{KCr}_3\text{As}_3\text{H}_{0.45}$. A strong magnetic shielding with MSF ($=4\pi\chi_{\text{ZFC}}$) over 100% (without the correction of demagnetization) can be seen at 2 K, while the magnetic expulsion fraction ($=4\pi\Delta\chi_{\text{FC}}$) is only about 0.4%, only 20% of the counterpart of $\text{K}_2\text{Cr}_3\text{As}_3$ polycrystals [1]. The superconducting onset transition temperature is 5.8 K, which is 1.1 K higher than that of the post-treated “ KCr_3As_3 ” crystals [20]. Meanwhile, the FC and ZFC curves start to bifurcate at 6.5 K, similar to the spin-glass transition in the aged or annealed samples [21]. Note that the samples before electrolysis do not show SC above 1.8 K, or only show trace SC with a MSF of 0.1%–0.3% (see Fig. S2 in the SM [24]). After the electrolysis even at room temperature (without annealing effect), superconductivity at 4.9 K emerges with a MSF of 100% (see Table S1 in the SM [24]). Therefore, the result directly demonstrates that H intercalation induces and enhances SC in the $\text{KCr}_3\text{As}_3\text{H}_x$ system.

Figure 5 shows the isothermal magnetization data for $\text{KCr}_3\text{As}_3\text{H}_{0.45}$. At 50 and 100 K, the field dependence of magnetization $M(H)$ is essentially linear. In the superconducting state at 1.8 K, an obvious magnetic hysteresis is seen in the low-field region, primarily due to superconducting magnetic-flux pinning. For $\mu_0 H > 2$ T, the $M_+(H)$ (with increasing magnetic field) and $M_-(H)$ (with decreasing magnetic field) data tend to merge together. The high-field $M(H)$ behaves as a Brillouin function, similar to the case in KCr_3As_3 polycrystals [17], suggesting existence of localized magnetic moments.

In order to address the magnetism in the normal state, we measured the temperature dependence of dc magnetic susceptibility under a higher magnetic field of $H = 10$ kOe. As shown in Fig. 6, the reciprocal of susceptibility $1/\chi(T)$ is essentially linear with temperature, indicating dominant CW paramagnetism, similar to that of the nonsuperconducting KCr_3As_3 [17]. The data fitting using the formula $\chi = \chi_0 + C/(T - \theta_{\text{CW}})$ yields $\chi_0 = 0.00090$ emu mol $^{-1}$, $C = 0.66$ emu K mol $^{-1}$, and $\theta_{\text{CW}} = -61$ K. From the C value, one obtains an effective magnetic moment of $2.30 \mu_B/\text{fu}$, equivalent to $1.33 \mu_B/\text{Cr}$. Note that the effective magnetic

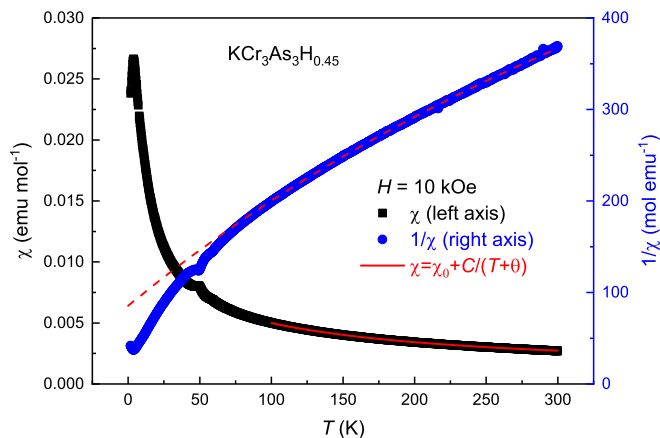


FIG. 6. Temperature dependence of magnetic susceptibility (left axis) and its reciprocal (right axis) for $\text{KCr}_3\text{As}_3\text{H}_{0.45}$. Red lines show the Curie-Weiss fitting. The small anomaly at around 50 K, commonly observed for porous samples exposed in air, is attributed to the antiferromagnetic transition of the residual condensed oxygen.

moment of nonsuperconducting KCr_3As_3 is merely $0.68 \mu_{\text{B}}/\text{Cr}$ [17]. Therefore, the Cr 3d electrons become more localized in the hydrogenized sample. It is generally acknowledged that a CW paramagnetism should not be the intrinsic property of a superconductor. Therefore, the CW paramagnetism is reasonably attributed to the spin-glassy phase, similar to the case of KCr_3As_3 polycrystals [17].

C. Specific heat

Figure 7 shows the specific-heat data, plotted with C/T vs T^2 , for the hydrogenized $\text{KCr}_3\text{As}_3\text{H}_{0.45}$. The data of nonsuperconducting KCr_3As_3 polycrystals [17] and superconducting 233-type $\text{K}_2\text{Cr}_3\text{As}_3$ [1] are also presented for a close comparison. The linear fit of the normal-

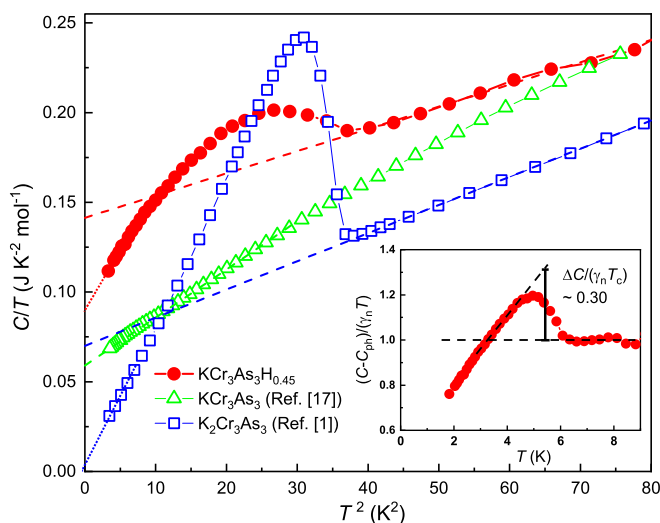


FIG. 7. Low-temperature specific-heat data for $\text{KCr}_3\text{As}_3\text{H}_{0.45}$, plotted in C/T vs T^2 . The data of superconducting $\text{K}_2\text{Cr}_3\text{As}_3$ and nonsuperconducting KCr_3As_3 are also presented for comparison. The lower inset shows temperature dependence of the electronic part ($C - C_{\text{ph}}$) scaled by $\gamma_n T$.

state data with the formula $C/T = \gamma_n T + \beta T^2$ gives $\gamma_n = 141 \text{ mJ K}^{-2} \text{ mol fu}^{-1} = 47 \text{ mJ K}^{-2} \text{ mol Cr}^{-1}$ and $\beta = 1.24 \text{ mJ K}^{-4} \text{ mol fu}^{-1}$. This electronic specific-heat constant γ_n is remarkably larger than those of KCr_3As_3 ($59 \text{ mJ K}^{-2} \text{ mol fu}^{-1}$ [17]) and $\text{K}_2\text{Cr}_3\text{As}_3$ ($70 \text{ mJ K}^{-2} \text{ mol fu}^{-1}$ [1]). The enhanced γ_n value suggests stronger electron correlations with the H intercalation. The Debye temperature $\theta_D = [(12/5)NR\pi^4/\beta]^{1/3} = 232 \text{ K}$ is slightly higher than that of $\text{K}_2\text{Cr}_3\text{As}_3$ (215 K) [1].

There is a broad specific-heat jump at the superconducting transition for $\text{KCr}_3\text{As}_3\text{H}_{0.45}$. By contrast, KCr_3As_3 does not show any sign of specific-heat anomaly, while $\text{K}_2\text{Cr}_3\text{As}_3$ shows a much sharper transition with a much larger jump. In particular, the C/T value at 1.8 K, the lowest temperature available in our experiments, remains $110 \text{ mJ K}^{-2} \text{ mol fu}^{-1}$ for $\text{KCr}_3\text{As}_3\text{H}_{0.45}$, and a rough linear extrapolation to zero temperature yields a residual $\gamma_0 = (C/T)_{T \rightarrow 0} \approx 90 \text{ mJ K}^{-2} \text{ mol fu}^{-1}$. For $\text{K}_2\text{Cr}_3\text{As}_3$, as a comparison, the C/T value at 1.8 K is only $30 \text{ mJ K}^{-2} \text{ mol fu}^{-1}$, and the extrapolated γ_0 is nearly zero. The result strongly suggests that a large portion of the $\text{KCr}_3\text{As}_3\text{H}_{0.45}$ sample is *not* superconducting. Assuming that the superconducting phase has the identical γ_n value, the electronic specific heat scaled by $\gamma_n T$ can be derived, which is plotted in the inset of Fig. 7. One sees that the dimensionless specific-heat jump $\Delta C/(\gamma_n T_c)$ is only 0.30, much less than the theoretical value (1.43) in the BCS weak-coupling scenario and the experimentally observed value (2.4) in $\text{K}_2\text{Cr}_3\text{As}_3$ [1]. With the former criterion, the superconducting volume fraction in $\text{KCr}_3\text{As}_3\text{H}_{0.45}$ is roughly estimated to be around 20%.

D. ^1H nuclear magnetic resonance

We observed an obvious ^1H NMR signal in both unhydrogenized and hydrogenized samples, confirming the H intercalation. The linewidth increases remarkably below $\sim 20 \text{ K}$ (Fig. S6 [24]), ruling out the possible origin of hydrogens from the solvent molecules such as H_2O and $\text{C}_2\text{H}_5\text{OH}$. As shown in the inset of Fig. 8(a), the total ^1H NMR spectrum of $\text{KCr}_3\text{As}_3\text{H}_{0.45}$ could be divided into two distinct parts, one sharp peak with larger integral area and one broad peak with smaller integral area. Further spin-lattice relaxation measurement on the frequency at the top of NMR spectrum indicates that there is also a two-component behavior in the T_1 process. As is clearly seen in Fig. 8(a), a two-component formula nicely fits the relaxation curve with one long T_1 and one short T_1 . Under 3-T field and at 7.3 K, the values of T_1^{long} and T_1^{short} are 23.5 and 0.86 s, respectively. The fitted result also indicates that the integral intensity for the long- T_1 component is larger than that for the short- T_1 component, suggesting a strong electronic inhomogeneity with the long- T_1 phase dominant in $\text{KCr}_3\text{As}_3\text{H}_{0.45}$.

Figure 8(b) plots the two sets of the $(T_1 T)^{-1}$ data as functions of temperature. In the high-temperature regime ($T > 10 \text{ K}$), both $(T_1 T)^{-1}$'s increase with decreasing temperature, suggesting existence of spin fluctuations. At lower temperatures, $(T_1^{\text{long}} T)^{-1}$ and $(T_1^{\text{short}} T)^{-1}$ drops at $\sim 9 \text{ K}$ and $\sim 5 \text{ K}$, respectively. Considering the weaker integral intensity and the similar transition temperature with the superconducting transition temperature of 5.8 K (note that T_c decreases a

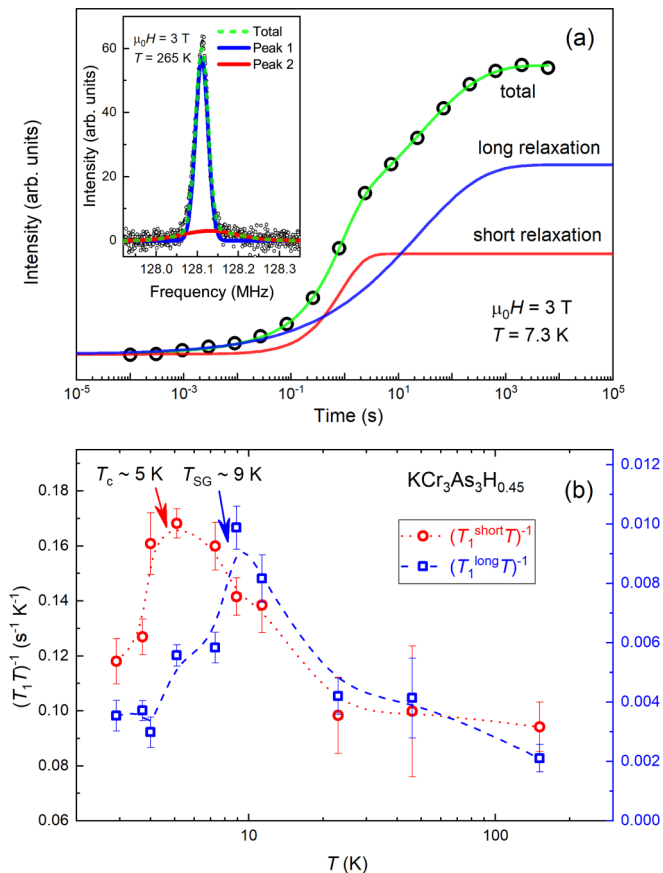


FIG. 8. ¹H NMR results for KCr₃As₃H_{0.45}. (a) Spin-lattice relaxation curve of ¹H nuclei and the corresponding data fitting with two components of T_1^{long} and T_1^{short} . Inset: ¹H NMR spectrum at 265 K with two-component fitting. Red and blue lines stand for two distinct fitting components and green dashed line stands for the total fitting curve. (b) Temperature dependence of $(T_1 T)^{-1}$ for both the long and short components.

little bit under a 3-T field), the drop in $(T_1^{\text{short}} T)^{-1}$ below ~ 5 K could be reasonably attributed to the minority superconducting phase in KCr₃As₃H_{0.45}. By contrast, the stronger integral intensity for T_1^{long} suggests its origin from the majority spin-glassy phase. Thus, the drop in $(T_1^{\text{long}} T)^{-1}$ should be ascribed to the majority spin-glassy phase. In addition, the spin-freezing temperature T_{SG} depends on the measurement frequency [17], the higher transition temperature in NMR measurement than that of the dc magnetic measurement above is probably due to the much higher frequency in the NMR measurement. In one word, the result of spin-lattice relaxation also supports a strong electronic inhomogeneity in KCr₃As₃H_{0.45}.

E. Discussion

Phase separation. The experimental results above demonstrate electronic inhomogeneity with a small fraction of superconducting phase in KCr₃As₃H_{0.45}. We have also learned from the XRD and EDS investigations that the inner part of the rodlike crystallites has better crystallinity where K deficiency is insignificant. Note that neutron diffraction study

shows a higher H content ($x \sim 0.7$ [22]), although the samples show a lower T_c and a lower MSF. This result suggests that the inner portion of the crystallites should have relatively high H content, and the outer part has lower H content. If this is the case, the inner part (minority phase) is probably responsible for SC and, accordingly, the outer part (majority phase) is the spin-glassy phase. As for the unhydrogenized sample, the electronic inhomogeneity also exists, as is revealed by the ¹H NMR spectrum [Fig. S8(b)]. In this circumstance, however, the two separated phases are both nonsuperconducting. Obviously, there should be a threshold of H content for the emergence of SC.

The above phase-separation scenario allows different H content (thus exhibiting different T_c) in the inner part of different crystallites, which explains the broad superconducting transition. It also explains why the H content measured by ¹H NMR is smaller than that of the neutron study: the former gives an overall H content and the latter only measures the H content of the inner part of the crystallites. Assuming that the fraction of superconducting phase is 20% (according to the specific-heat data analysis above), and taking the H content of the nonsuperconducting phase as 0.35 [24], one can easily estimate that the H content of the superconducting phase is 0.85 in the KCr₃As₃H_{0.45} sample. This value of H content is significantly higher than that of neutron-diffraction result, which accounts for the higher T_c observed in this study. By this logic, one could expect that bulk SC with an even higher T_c could be realized in the fully hydrogenized compound KCr₃As₃H.

Electron localization and correlation. The hydrogenization in KCr₃As₃H_x not only induces or enhances SC, but also significantly changes other physical properties of the system, as shown in Table II. First, the spin-glass transition temperature increases with the H intercalation, in the same tendency as the superconducting transition temperature does. The result implies that both the spin freezing and SC share a similar mechanism, i.e., exchange interactions of spins.

Second, the nonsuperconducting spin-glassy phase shows an enhanced effective localized moment from 0.68 μ_B/Cr in KCr₃As₃ to 1.33 μ_B/Cr in KCr₃As₃H_{0.45}. If $\sim 20\%$ superconducting phase (which does not contribute the CW paramagnetism) is taken out, the effective moment should turn out to be 1.48 μ_B/Cr for the nonsuperconducting phase, which is close to the theoretical value of 1.73 μ_B/Cr for spin $\frac{1}{2}$. This means more Cr-3d electrons become localized.

Third, the overall electronic specific-heat coefficient increases from 20 mJ K⁻² mol Cr⁻¹ in KCr₃As₃ to 47 mJ K⁻² mol Cr⁻¹ in KCr₃As₃H_{0.45}. The enhancement of γ_n suggests stronger correlations for the itinerant electrons in the hydrogenized sample. In the 233-type system, T_c is nearly proportional to γ_n [7]. It also seems to be true that stronger electron correlations with higher γ_n may give rise to a higher T_c in the KCr₃As₃H_x system.

The enhanced localized moment of the nonsuperconducting phase and the enhanced electronic specific-heat coefficient in the superconducting phase are both likely attributed to the expansion and/or distortion of the Cr octahedra in the Cr₃ chains. The structure change may lead to energy band narrowing, which possibly gives rise to electronic localization as well as stronger electron correlations.

IV. CONCLUDING REMARKS

In summary, we have directly demonstrated that SC can be induced or enhanced in the 133-type $K_{1-\delta}Cr_3As_3H_x$ via electrochemical hydrogenation. With an average H content of about 0.45, the T_c value achieves a record high of 5.8 K in the K-Cr-As-H system. Nevertheless, the superconducting volume fraction is only about 20%. The dominant nonsuperconducting phase possesses a CW paramagnetism with enhanced effective magnetic moment. It is likely that the inner part of the rodlike crystallites bears a higher H content, which is responsible for the SC observed. If more hydrogen could be intercalated, one would expect bulk SC in H-rich $KCr_3As_3H_x$.

We also found that the hydrogenation in $KCr_3As_3H_x$ system leads to significant expansions and distortions of the Cr

octahedra in the Cr_3 chains. The structural changes may give rise to stronger electron correlations and stronger electron localizations, which could be the reason for the enhanced electronic specific-heat coefficient in the superconducting phase and the enhanced localized moment for the nonsuperconducting phase. Future study with first-principles calculations is expected to clarify this interesting issue.

ACKNOWLEDGMENTS

This work was supported by National Natural Science Foundation of China (Grant No. 11674281) and National Key Research and Development Program of China (Grants No. 2017YFA0303001 and No. 2017YFA0303002), Fundamental Research Funds for the Central Universities of China.

-
- [1] J.-K. Bao, J.-Y. Liu, C.-W. Ma, Z.-H. Meng, Z.-T. Tang, Y.-L. Sun, H.-F. Zhai, H. Jiang, H. Bai, C.-M. Feng, Z.-A. Xu, and G.-H. Cao, Superconductivity in Quasi-One-dimensional $K_2Cr_3As_3$ with Significant Electron Correlations, *Phys. Rev. X* **5**, 011013 (2015).
- [2] W. Wu, J. Cheng, K. Matsubayashi, P. Kong, F. Lin, C. Jin, N. Wang, Y. Uwatoko, and J. Luo, Superconductivity in the vicinity of antiferromagnetic order in CrAs, *Nat. Commun.* **5**, 5508 (2014).
- [3] T. Kong, S. L. Bud'ko, and P. C. Canfield, Anisotropic H_{c2} , thermodynamic and transport measurements, and pressure dependence of T_c in $K_2Cr_3As_3$ single crystals, *Phys. Rev. B* **91**, 020507(R) (2015).
- [4] Y. T. Shao, X. X. Wu, L. Wang, Y. G. Shi, J. P. Hu, and J. L. Luo, Evidence of line nodes in superconducting gap function in $K_2Cr_3As_3$ from specific-heat measurements, *Europhys. Lett.* **123**, 57001 (2018).
- [5] W. Wu, X. Zhang, Z. Yin, P. Zheng, N. Wang, and J. Luo, Low temperature properties of pnictide CrAs single crystal, *Sci. China-Phys. Mech. Astron.* **53**, 1207 (2010).
- [6] H. Jiang, G. Cao, and C. Cao, Electronic structure of quasi-one-dimensional superconductor $K_2Cr_3As_3$ from first-principles calculations, *Sci. Rep.* **5**, 16054 (2015).
- [7] G.-H. Cao, J.-K. Bao, Z.-T. Tang, Y. Liu, and H. Jiang, Peculiar properties of Cr_3As_3 -chain-based superconductors, *Philos. Mag.* **97**, 591 (2017).
- [8] R. Y. Chen and N. L. Wang, Progress in Cr- and Mn-based superconductors: A key issues review, *Rep. Prog. Phys.* **82**, 012503 (2018).
- [9] X. Wu, F. Yang, C. Le, H. Fan, and J. Hu, Triplet p_z -wave pairing in quasi-one-dimensional $A_2Cr_3As_3$ ($A = K, Rb, Cs$), *Phys. Rev. B* **92**, 104511 (2015).
- [10] Y. Zhou, C. Cao, and F.-C. Zhang, Theory for superconductivity in alkali chromium arsenides $A_2Cr_3As_3$ ($A = K, Rb, Cs$), *Sci. Bull.* **62**, 208 (2017).
- [11] H. Zhong, X.-Y. Feng, H. Chen, and J. Dai, Formation of Molecular-Orbital Bands in a Twisted Hubbard Tube: Implications for Unconventional Superconductivity in $K_2Cr_3As_3$, *Phys. Rev. Lett.* **115**, 227001 (2015).
- [12] J. Yang, Z. T. Tang, G. H. Cao, and G.-q. Zheng, Ferromagnetic Spin Fluctuation and Unconventional Superconductivity in $Rb_2Cr_3As_3$ Revealed by As-75 NMR and NQR, *Phys. Rev. Lett.* **115**, 147002 (2015).
- [13] J. Luo, J. Yang, R. Zhou, Q. G. Mu, T. Liu, Z.-a. Ren, C. J. Yi, Y. G. Shi, and G.-q. Zheng, Tuning the Distance to a Possible Ferromagnetic Quantum Critical Point in $A_2Cr_3As_3$, *Phys. Rev. Lett.* **123**, 047001 (2019).
- [14] Z.-T. Tang, J.-K. Bao, Y. Liu, Y.-L. Sun, A. Ablimit, H.-F. Zhai, H. Jiang, C.-M. Feng, Z.-A. Xu, and G.-H. Cao, Unconventional superconductivity in quasi-one-dimensional $Rb_2Cr_3As_3$, *Phys. Rev. B* **91**, 020506(R) (2015).
- [15] Z.-T. Tang, J.-K. Bao, Z. Wang, H. Bai, H. Jiang, Y. Liu, H.-F. Zhai, C.-M. Feng, Z.-A. Xu, and G.-H. Cao, Superconductivity in quasi-one-dimensional $Cs_2Cr_3As_3$ with large interchain distance, *Sci. China Mater.* **58**, 16 (2015).
- [16] Q.-G. Mu, B.-B. Ruan, B.-J. Pan, T. Liu, J. Yu, K. Zhao, G.-F. Chen, and Z.-A. Ren, Ion-exchange synthesis and superconductivity at 8.6 K of $Na_2Cr_3As_3$ with quasi-one-dimensional crystal structure, *Phys. Rev. Mater.* **2**, 034803 (2018).
- [17] J.-K. Bao, L. Li, Z.-T. Tang, Y. Liu, Y.-K. Li, H. Bai, C.-M. Feng, Z.-A. Xu, and G.-H. Cao, Cluster spin-glass ground state in quasi-one-dimensional KCr_3As_3 , *Phys. Rev. B* **91**, 180404(R) (2015).
- [18] Z.-T. Tang, J.-K. Bao, Y. Liu, H. Bai, H. Jiang, H.-F. Zhai, C.-M. Feng, Z.-A. Xu, and G.-H. Cao, Synthesis, crystal structure and physical properties of quasi-one-dimensional ACr_3As_3 ($A = Rb, Cs$), *Sci. China Mater.* **58**, 543 (2015).
- [19] Y. Feng, X. Zhang, Y. Hao, A. D. Hillier, D. T. Adroja, and J. Zhao, Magnetic ground state of KCr_3As_3 , *Phys. Rev. B* **99**, 174401 (2019).
- [20] Q.-G. Mu, B.-B. Ruan, B.-J. Pan, T. Liu, J. Yu, K. Zhao, G.-F. Chen, and Z.-A. Ren, Superconductivity at 5 K in quasi-one-dimensional Cr-based KCr_3As_3 single crystals, *Phys. Rev. B* **96**, 140504(R) (2017).
- [21] J.-J. Xiang, Y.-L. Yu, S.-Q. Wu, B.-Z. Li, Y.-T. Shao, Z.-T. Tang, J.-K. Bao, and G.-H. Cao, Superconductivity induced by aging and annealing in $K_{1-\delta}Cr_3As_3H_x$, *Phys. Rev. Mater.* **3**, 114802 (2019).
- [22] K. M. Taddei, L. D. Sanjeeva, B.-H. Lei, Y. Fu, Q. Zheng, D. J. Singh, A. S. Sefat, and C. de la Cruz, Tuning

- from frustrated magnetism to superconductivity in quasi-one-dimensional KCr_3As_3 through hydrogen doping, *Phys. Rev. B* **100**, 220503(R) (2019).
- [23] S.-Q. Wu, C. Cao, and G.-H. Cao, Lifshitz transition and nontrivial H-doping effect in the Cr-based superconductor $\text{KCr}_3\text{As}_3\text{H}_x$, *Phys. Rev. B* **100**, 155108 (2019).
- [24] See Supplemental Material at <http://link.aps.org/supplemental/10.1103/PhysRevMaterials.4.124802> for additional experimental data (with nine figures and one table) including details of the electrolysis and the H-content analysis.
- [25] F. Izumi and K. Momma, Three-dimensional visualization in powder diffraction, *Solid State Phenom.* **130**, 15 (2007).
- [26] Y. Liu, J.-K. Bao, H.-K. Zuo, A. Ablimit, Z.-T. Tang, C.-M. Feng, Z.-W. Zhu, and G.-H. Cao, Effect of impurity scattering on superconductivity in $\text{K}_2\text{Cr}_3\text{As}_3$, *Sci. China-Phys. Mech. Astron.* **59**, 657402 (2016).
- [27] T. Liu, Q.-G. Mu, B.-J. Pan, J. Yu, B.-B. Ruan, K. Zhao, G.-F. Chen, and Z.-A. Ren, Superconductivity at 7.3 K in the 133-type Cr-based RbCr_3As_3 single crystals, *Europhys. Lett.* **120**, 27006 (2017).